CHEMISTRY OF MATERIALS
Article

Chem. Mater. **2010,** *22,* 2315–2324 2315
DOI:10.1021/cm9032622

Hydrothermal Yb^{3+}-Doped $NaGd(WO_4)_2$ Nano- and Micrometer-Sized Crystals with Preserved Photoluminescence Properties

Fátima Esteban-Betegón, Carlos Zaldo, and Concepción Cascales*

Instituto de Ciencia de Materiales de Madrid, Consejo Superior de Investigaciones Científicas. c/Sor Juana Inés de la Cruz, 3, E-28049 Madrid, Spain

Received October 23, 2009. Revised Manuscript Received February 2, 2010

Mild hydrothermal preparations using nitrate and chloride reagents as Gd^{3+} and Yb^{3+} sources lead to the synthesis of $NaGd_{1-x}Yb_x(WO_4)_2$ ($0.001 \leq x \leq 0.5$) particles with tetragonal scheelite-like structure phase. Nearly neutral pH ~7.5 conditions ensure the stability of this crystalline phase over a wide range of reaction times. Synthetical routes with both kind of reagents yield basically the same particle morphology sequences, although using Gd(Yb)-chlorides the presence of nanorods is more evident, whereas using Gd(Yb)-nitrates the faster growth rate favors well-defined micrometer-sized octahedral particles. The spectroscopic properties of Yb^{3+} in $NaGd_{1-x}Yb_x(WO_4)_2$ synthesized micrometer-sized octahedra are equivalent to those obtained in bulk single crystals, showing a single exponential photoluminescence decay and $^2F_{5/2}$ lifetime $\tau \approx 330$ μs for $0.001 \leq x \leq 0.005$ doped samples. The nanoparticles and nanorods formed with Gd(Yb)-nitrates and pH < 7 by short time annealing as well as in Gd(Yb)-chloride preparations show a strong reduction of the Yb^{3+} lifetime with regards to that observed in micrometer-sized octahedra or in single crystals, leading to nonexponential fluorescence decays when both nano- and micrometer-sized particles coexist. The use of raw Yb_2O_3 with increasing purity level in the hydrothermal process yields materials that show an increase in Yb^{3+} lifetime toward its radiative value.

Introduction

With the development of infrared diode lasers for optical pumping, the preparation of Yb^{3+}-doped laser media became a matter of major interest in the current solid-state laser technology, especially for high power applications in diode-pumped thin disk,[1] waveguide,[2] and fiber[3] design configurations. Main reasons sustaining this interest are the availability of affordable and high-power InGaAs diode lasers emitting at 980 nm, where Yb^{3+} has rather high optical absorption, and the small quantum defect[4] characteristic for the absorption and emission processes associated to the $4f^{13}$ electronic configuration of Yb^{3+}, which minimizes the heat transfer to the host. Furthermore, Yb^{3+} exhibits a significant broadening of its optical transitions, which makes it suitable for tunable lasers and for ultrashort pulse operation. This broadening can be enhanced by the local structural disorder provided by the crystal host. An important class of these disordered materials are the tetragonal scheelite-related double tungstates with nominal formula $MT(WO_4)_2$, where M is a monovalent cation, like the alkaline ones and Ag^+, and T is a trivalent cation, including Bi^{3+}, Y^{3+}, La^{3+} and all lanthanides. Over the last years CW tunable laser operation has been shown in Yb-doped $NaY(WO_4)_2$,[5] $NaLa(WO_4)_2$,[6,7] $NaGd(WO_4)_2$,[8,9] and $NaLu(WO_4)_2$[10] crystals as well as in other isostructural double molybdates like $NaLa(MoO_4)_2$[11] and $LiGd(MoO_4)_2$,[12] and recently, efficient mode-locked 53 fs laser

*To whom correspondence should be addressed. E-mail ccascales@icmm.csic.es.

(1) Petermann, K.; Fagundes-Peters, D.; Johannsen, J.; Mond, M.; Peters, V.; Romero, J. J.; Kutovoi, S.; Speiser, J.; Giesen, A. *J. Cryst. Growth* **2005**, *275*, 135.
(2) Shepherd, D. P.; Hettrick, S. J.; Li, C.; Mackenzie, J. I.; Beach, R. J.; Mitchell, S. C.; Meissner, H. E. *J. Phys. D: Appl. Phys.* **2001**, *34*, 2420.
(3) Kim, D.; Soh, B. S.; Nilsson, J.; Richardson, D. J.; Sahu, J. K. *IEEE J. Sel. Top. Quantum Electron.* **2007**, *13*, 588.
(4) García-Cortés, A.; Zaldo, C.; Cascales, C.; Mateos, X.; Petrov, V. *Opt. Express* **2007**, *15*, 18162.
(5) García-Cortés, A.; Cano-Torres, J. M.; Serrano, M. D.; Cascales, C.; Zaldo, C.; Rivier, S.; Mateos, X.; Griebner, U.; Petrov, V. *IEEE J. Quantum Electron.* **2007**, *43*, 758.
(6) Liu, J.; Cano-Torres, J. M; Cascales, C.; Esteban-Betegón, F.; Serrano, M. D; Volkov, V.; Zaldo, C.; Rico, M.; Griebner, U.; Petrov, V. *Phys. Status Solidi, A* **2005**, *202*, R29.
(7) Liu, J.; Cano-Torres, J. M.; Esteban-Betegón, F.; Serrano, M. D.; Cascales, C.; Zaldo, C.; Rico, M.; Griebner, U.; Petrov, V. *Opt Laser Technol.* **2007**, *39*, 558.
(8) Cascales, C.; Serrano, M. D.; Esteban-Betegón, F.; Zaldo, C.; Peters, R.; Petermann, K.; Huber, G.; Ackermann, L.; Rytz, D.; Dupré, C.; Rico, M.; Liu, J.; Griebner, U.; Petrov, V. *Phys. Rev. B* **2006**, *74*, 174114.
(9) Rico, M.; Liu, J; Griebner, U.; Petrov, V.; Serrano, M. D.; Esteban-Betegón, F.; Cascales, C.; Zaldo, C. *Opt. Express* **2004**, *12*, 5362.
(10) García-Cortés A., Cano-Torres J. M., Han X, Cascales C., Zaldo C., Mateos X., Rivier S., Griebner U., Petrov V. Valle F. J. *J. Appl. Phys.* **2007**, *101*, 063110:1−7.
(11) Rico, M.; Liu, J.; Cano-Torres, J. M.; García-Cortés, A.; Cascales, C.; Zaldo, C.; Griebner, U.; Petrov, V. *Appl. Phys. B: Laser Opt.* **2005**, *81*, 621.
(12) Rico, M.; Griebner, U.; Petrov, V.; Ortega, P.; Han, X.; Cascales, C.; Zaldo, C. *J. Opt. Soc. Am., B* **2006**, *23*, 1083.

Published on Web 02/17/2010

pulses at $\lambda \approx 1035$ nm have been obtained with Yb-doped $NaY(WO_4)_2$ bulk crystals.[5]

Unfortunately, the thermal conductivity of single crystals of tetragonal scheelite-related double tungstates and molybdates is relatively low, 1.5−2 W m^{-1} K^{-1}, limiting power applications. Therefore, it is required to incorporate them in hybrid composites to allow a more efficient cooling of the optical medium. A first step in this direction is the synthesis of nanocrystalline particles with size and morphologies suitable for infiltration or merging with other materials also transparent in the infrared. Diverse methodologies including solution combustion,[13] coprecipitation,[14] and microwave assisted processes[15,16] have been extensively applied to prepare nanocrystals of tetragonal scheelite DWO_4 (D = Ba^{2+}, Ca^{2+}, Ni^{2+}, Sr^{2+}) phases, which although attractive still face issues in efficient control over the crystal size, morphology, and composition, aspects that are crucial for high luminescence performance. Mild hydrothermal (hereafter HT) processes benefit not only from much lower temperatures than other preparation methods but also from being advantageous for homogeneous nucleation of nanocrystals with well-defined morphologies. However, along with other obvious benefices provided by HT reactions, as the softer environment and scalability, the possible presence of adsorbed and/or occluded water and/or adsorbed atmospheric CO_2 in the surface of the prepared nanocrystals can originate an important nonradiative deactivation, leading to lower emission efficiencies when compared to the high-temperature prepared bulk single-crystals counterparts.[17]

The first objective of the work is the comprehensive study of the effects of starting reagents, solution pH, temperature, and reaction time upon the resulting products of the HT synthesis of the Yb-doped $NaGd(WO_4)_2$ tetragonal scheelite-related phase, that is, the determination of the stability range, morphology, and size of the optically active materials that can be obtained under different preparative conditions. This survey is carried out to elucidate the softest reaction conditions, namely the best combination for lowest required temperature and minimum reaction time while keeping the reaction medium close to pH neutrality, yielding a micro- or nanocrystalline material with suitable characteristics to prepare hybrid laser active composites by infiltration or merging. The next aspect to be considered is the evaluation of the relationship of the emission properties with the morphology and size of the HT Yb-$NaGd(WO_4)_2$ material, as well as with the Yb^{3+} concentration. Proper comparisons with corresponding data from counterpart bulk single crystals[8,9] will allow establishing the most adequate way to prepare HT Yb-$NaGd(WO_4)_2$ with reduced energy losses at surface defects, and thus with higher luminescence efficiency. Furthermore, to rationalize the effect of the luminescence quenching by nonradiative losses to possible impurities[18,19] (mainly Er^{3+} and Tm^{3+}), the $^2F_{5/2}$ Yb^{3+} fluorescence lifetime of several HT $NaGd_{1-x}Yb_x(WO_4)_2$ compositions ($0.001 \leq x \leq 0.5$, i.e., Yb^{3+} concentration [Yb] from 0.1 to 50 mol %) has been determined in series prepared using from medium (99.9%) to ultrapure (99.9999%) Yb_2O_3 oxide as the starting reagent.

Experimental Section

Sample Preparation. Sets of Yb-doped $NaGd_{1-x}Yb_x(WO_4)_2$ (x = 0.001, 0.002, 0.005, 0.01, 0.02, 0.05, 0.10, 0.15, 0.25, 0.50) samples have been hydrothermally prepared using as reactants $Na_2WO_4 \times 2H_2O$ (Strem Chemicals, 99.9%), and either nitrates or chlorides as the lanthanide (RE) source. The procedure with nitrates ($Gd(NO_3)_3 \times 6H_2O$, $Yb(NO_3)_3 \times 5H_2O$, Strem Chemicals, 99.99%, hereafter shortly Gd(Yb)-NIT) consists in the dissolution in distilled water of the corresponding stoichiometric molar amounts of nitrates, and after this $Na_2WO_4 \times 2H_2O$ is slowly added with vigorous magnetic stirring. The formed white suspension of amorphous particles is then stirred continuously for 10 min, the pH adjusted to 5, 6, 7.0−7.5, and 13 by adding diluted HNO_3 or alternatively NaOH solutions, and subsequently heated to temperatures of 170 °C (for compositions with $0.001 \leq x \leq 0.05$), 185 °C ($0.10 \leq x \leq 0.25$), and 200 °C ($x = 0.50$) in Teflon-lined autoclaves of 75 mL capacity. Reactions with times lasting from 3 to 14 h have been carried out. In each case, the white precipitate is repeatedly washed with distilled water and separated by centrifugation, and finally dried at 110 °C.

In the synthesis route with chlorides (hereafter Gd(Yb)-CHL) the starting sesquioxides Gd_2O_3 (WuXi YiFeng Rare Earth Co Ltd., 99.99%) and Yb_2O_3 (99.9% Strem Chemicals, 99.99% WuXi YiFeng Rare Earth Co Ltd., 99.998% and 99.9999% Alfa Aesar) are dissolved under heating with agitation in dilute HCl solution (10 mL distilled water and 5 mL 38 wt % HCl). After complete evaporation, 20 mL of distilled water is added to form a clear solution, and then mixed with the 20 mL transparent solution of $Na_2WO_4 \times 2H_2O$ to form the white suspension. The process continues in the same way as previously indicated for nitrates.

Characterization of Hydrothermal (HT) Samples. The purity of the required tetragonal phase was in each case tested by 300 K powder X-ray diffraction (XRPD) performed in a Bruker AXS D-8 Advance diffractometer, using Cu K_α radiation.

Thermal analyses were made by differential scanning calorimetry (DSC) in a Setaram SetSys Evolution 1700 DTG-DSC system. Amounts of ~50 mg were heated in argon up to 900 °C at a scanning rate of 10 °C min^{-1}.

Field-emission scanning electron microscopy (FE-SEM) images were taken with a FEI NOVA SEM230 microscope with

(13) Tessari, G.; Bettinelli, M.; Speghini, A.; Ajo, D.; Pozza, G.; Depero, L. E.; Allieri, B.; Sangaletti, L. *Appl. Surf. Sci.* **1999**, *144−145*, 686.
(14) Zhao, X.; Li, T.; Xi, Y.; Ng, D. H. L.; Yu, J. *Cryst. Growth &Design* **2006**, *6*, 2210.
(15) Ryu, J. H.; Yoon, J. W.; Lim, C. S.; Oh, W. C.; Shim, K. B. *Ceram. Int.* **2005**, *31*, 883.
(16) Thongtem, T.; Phuruangrat, A.; Thongtem, S. *Curr, Appl. Phys.* **2008**, *8*, 189.
(17) Capobianco, J. A.; Boyer, J. C.; Vetrone, F.; Speghini, A.; Bettinelli, M. *Chem. Mater.* **2002**, *14*, 2915.
(18) Müller, V.; Peters, V.; Heumann, E.; Henke, M.; Petermann, K.; Huber, G. Growth, characterization, and laser operation of $Yb_3Al_5O_{12}$ with nearly intrinsic Yb^{3+}-fluorescence lifetime. In *Proceedings of the Advanced Solid-State Laser Topical Meeting*; Quebec, Feb 2−6, 2002; Optical Society of America: Washington, D.C., 2002; pp 153−155
(19) Peters, R.; Kränkel, C.; Petermann, K.; Huber, G. *J. Cryst. Growth* **2008**, *310*, 1934.

an accelerating voltage of 5−7 kV. Transmission electron microscopy (TEM) images were recorded with a JEOL 2000FXII microscope with an accelerating voltage of 200 kV. High resolution TEM (HRTEM) images were obtained with a JEOL model JEM-4000 EX microscope, with an accelerating voltage of 400 kV.

Fourier transform infrared absorption (FT-IR) data were collected on a Nicolet 20SXC spectrophotometer in the range 4000−400 cm^{-1}, and KBr was used to prepare pellets of the analyzed materials.

Yb^{3+} fluorescence was excited with a Quanta-Ray MOPO-HF optical parametric oscillator. This system provides laser pulses shorter than 10 ns from 440 to 680 nm and from 730 to 1750 nm. The pulse energy was ∼25 mJ for λ = 940 nm. The fluorescence was dispersed by a single grating SPEX spectrometer (f = 34 cm) and measured by a Hamamatsu InP/InGaAs cooled photomultiplier, model H9170−75, sensitive in the 950−1700 nm range. The electrical signals were recorded either with a lock-in amplifier for emission and excitation spectra or with a Tektronix oscilloscope, model TDS-520, for lifetime measurements. For these measurements HT synthesized materials were dispersed in two fluid media, ethylene glycol (EG), with refractive index n = 1.52, or poly(chlorotrifluoroethylene) also know as Fluorolube (FL), with n = 1.94. Both media are transparent in the near-infrared region used for Yb^{3+} characterization.

Results and Discussion

Range of Stability for the Tetragonal Yb-Doped NaGd-$(WO_4)_2$. *A. Effects of the pH and Reaction Time on the Formation of the Phase*. XRPD patterns of HT samples prepared from Gd(Yb)-NIT with nominal composition $NaGd_{0.95}Yb_{0.05}(WO_4)_2$ at 170 °C, and different controlled pH and reaction time conditions are shown in Figure 1a−d. It can be observed that the pH of the initial mixed dispersion plays a crucial role in the formation of the searched tetragonal phase. With pH 5, Figure 1a, the products of HT treatment after 3 h (Figure 1a1) and 6 h (Figure 1a2) are still amorphous, and even prolonged reactions until 14 h (Figure 1a3) do not yield the scheelite-like phase. Upon raising the pH to 6, Figure 1b, the characteristic diffraction peaks of the tetragonal Yb-NaGd-$(WO_4)_2$ phase[8,20] evolve gradually from the initially amorphous material, and although after 6 h the material is mostly constituted by the scheelite phase, only within a limited range of reaction times this pure crystalline phase is reached, i.e., not less than 9 h but longer reactions (14 h and over) are detrimental. For samples obtained with pH 7.5, Figure 1c, the pure tetragonal Yb-$NaGd(WO_4)_2$ phase appears with 8 h of thermal treatment being maintained without decomposition after prolonged reactions. Although shorter times produce amorphous materials for both pH 6 and 7.5, they seem to be different, being in the first case a true precursor of the crystalline tetragonal $NaGd(WO_4)_2$ phase, whereas no similarity is shown for the latter. Finally, in highly basic conditions, pH 13−14, see Figure 1d, the reaction products after 5−12 h are always the mixture of well-crystallized Na_2WO_4[21] and hexagonal $Gd(OH)_3$.[22] To facilitate the identification of Bragg reflections corresponding to the tetragonal scheelite

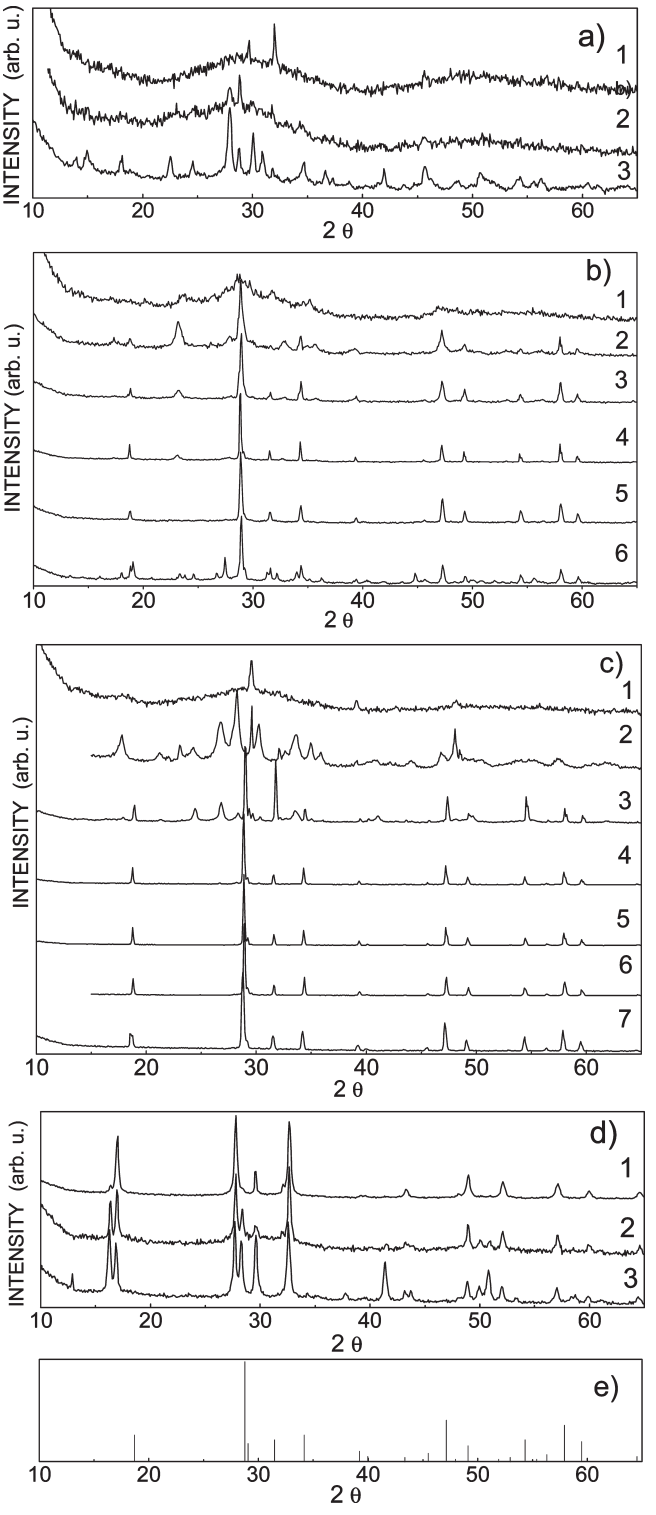

Figure 1. Room-temperature X-ray diffraction patterns of $NaGd_{0.95}Yb_{0.05}(WO_4)_2$ synthesized in hydrothermal treatments at 170 °C using Gd(Yb)-NIT and different pH values and reaction times t: (a) pH 5 and t = 3 h (1), t = 6 h (2), and t = 14 h (3); (b) pH 6 and t = 3 h (1), t = 4 h (2), t = 6 h (3), t = 8 h (4), t = 9 h (5), and t = 14 h (6); (c) pH 7.5, t = 0 h (without hydrothermal treatment) (1), t = 2 h (2), t = 7 h (3), t = 8 h (4), t = 9 h (5), t = 12 h (6), and t = 14 h (7); (d) pH 13 and t = 5 h (1), t = 7 h (2), and t = 12 h (3); (e) X-ray diffraction pattern scheme for $NaGd(WO_4)_2$ (JCPDS File 25−0829).

(20) *Collection Code 156473 of Inorganic Crystal Structure Database*; Fachinformationszentrum (FIZ) Karlsruhe: Eggenstein-Leopolshafen, Germany, 2009.

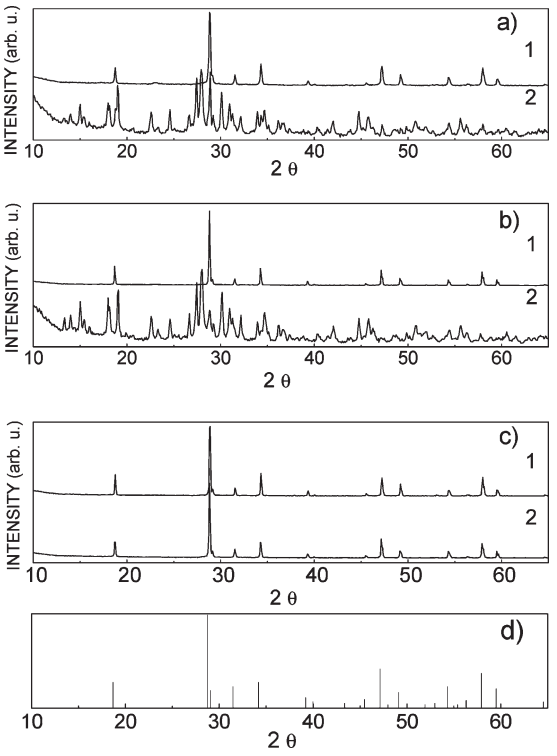

Figure 2. Room-temperature X-ray diffraction patterns of $NaGd_{0.95}Yb_{0.05}(WO_4)_2$ synthesized in hydrothermal treatments at 170 °C using Gd(Yb)-CHL and different pH values and reaction times *t*: (a) pH 6, and $t = 8$ h (1), $t = 12$ h (2); (b) pH 7, and $t = 8$ h (1), $t = 12$ h (2); (c) pH 7.5, and $t = 8$ h (1), $t = 14$ h (2); (d) X-ray diffraction pattern scheme for $NaGd(WO_4)_2$ (JCPDS card 25−0829).

phase, Figure 1e shows the X-ray diffraction pattern scheme for $NaGd(WO_4)_2$ (JCPDS File Nr. 25−0829).[23]

B. Effect of the Composition of the Used RE-Reactant on the Formation of the Phase. When using Gd(Yb)-NIT as reactants the former exploration discards the need of synthesis conditions at the wing sides of the pH scale for the preparation of pure tetragonal Yb-doped $NaGd(WO_4)_2$ samples, that is, the most favorable conditions correspond to the pH range from slight acidity to near neutrality in the starting dispersions. Thus, a second step is a parallel analysis of the evolution of the obtained crystal phase with the reaction time by using Gd(Yb)-CHL, but now it will be performed only in the above indicated pH range. Figure 2a−c displays XRPD patterns that summarize the results. Using pH 6.0 and pH 7.0 solutions, HT treatments at 170 °C lasting 8 h yielded, in both cases, pure crystalline $NaGd_{0.95}Yb_{0.05}(WO_4)_2$, see a1 and b1 in Figure 2, although the crystal phase is not maintained when the reaction is prolonged to 12 h, as can be seen in Figure 2a2 and Figure 2b2. However, some increase of the pH up to ~7.5 allows obtaining the pure tetragonal phase after longer reaction times, see Figure 2c.

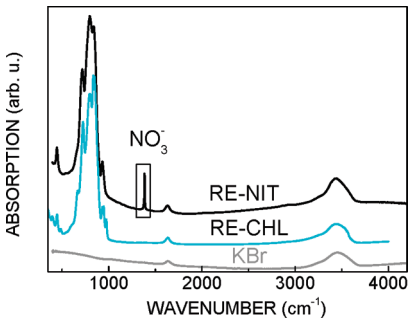

Figure 3. Room-temperature FT-IR spectra of $NaGd_{0.95}Yb_{0.05}(WO_4)_2$ prepared at $T = 170$ °C, pH 7.5 and $t = 8$ h, from RE-nitrates (black line) and RE-chlorides (cyan line). The spectrum of KBr used for preparing pellets (gray line) is shown for reference.

Figure 2d shows the X-ray diffraction pattern scheme for $NaGd(WO_4)_2$ (JCPDS File 25−0829).[23]

C. Reaction Temperature and Ytterbium Concentration in Tetragonal $NaGd_{1-x}Yb_x(WO_4)_2$ Series. The above results correspond to the preparation of samples from both Gd(Yb)-NIT or -CHL reactants with a unique Yb^{3+} doping concentration, namely $NaGd_{0.95}Yb_{0.05}(WO_4)_2$. XRPD analyses of the products of HT treatments corresponding to the preparation of samples with Yb^{3+} concentration in the range $0.001 \leq x \leq 0.5$ (i.e., from 0.1 mol % to 50 mol % Yb^{3+}) reveal that the minimum required temperature to obtain the pure and well-crystallized tetragonal phase is getting higher when increasing the Yb content. Thus, temperatures of 160−170 °C ($0.001 \leq x \leq 0.05$), 185 °C ($0.10 \leq x \leq 0.25$) and 200 °C ($x = 0.50$) are needed to yield the pure tetragonal phase in 8−9 h HT treatments of both Gd(Yb)-NIT and -CHL derived materials, although a finer, continuously increased temperature tuning would be envisaged.

Unit-cell parameters determined from Rietveld refinements of the corresponding XRPD profiles show a monotonic decrease with the Yb^{3+} incorporation in the $NaGd(WO_4)_2$ host. For the CHL series they are ranging from $a = 5.247(1)$ Å and $c = 11.377(2)$ Å to $a = 5.216(1)$ Å and $c = 11.316(2)$ Å for $x = 0.001$ to $x = 0.5$. The stoichiometric $NaYb(WO_4)_2$ material has been unable to be prepared since the required temperature of the reaction surpassed the stable working temperature of the Teflon containers.

To further evaluate possible differences in HT samples prepared by using either Gd(Yb)-NIT or -CHL as the RE source, we have collected for the same composition the corresponding room-temperature FT-IR spectra. The Figure 3 shows these spectra for $NaGd_{0.95}Yb_{0.05}(WO_4)_2$, chosen as the representative example, together with the spectrum of a blank KBr pellet. For both preparations (with fixed temperature T, pH, and reaction time *t* of 170 °C, 7.5, and 8 h, respectively) bands observed from ~400 to 960 cm^{-1} are basically the same described and assigned to modes of skeletal vibrations and modes originated from WO_4^{2-} internal vibrations in $NaGd(WO_4)_2$,[24] being the typical frequencies quoted for the

(21) *Powder Diffraction File 74−2369, PCPDFWin v. 2.2*; Joint Committee on Powder Diffraction Standards, International Centre for Diffraction Date: Newtown Square, PA, 2001.
(22) *Powder Diffraction File 83−2037, PCPDFWin v. 2.2*; Joint Committee on Powder Diffraction Standards, International Centre for Diffraction Date: Newtown Square, PA, 2001.
(23) *Powder Diffraction File 25−0829, PCPDFWin v. 2.2*; Joint Committee on Powder Diffraction Standards, International Centre for Diffraction Date: Newtown Square, PA, 2001.
(24) Perets, S.; Shneck, R. Z.; Gajic, R.; Golubovic, A.; Burshtein, Z. *Vib. Spectrosc.* **2009**, *49*, 110.

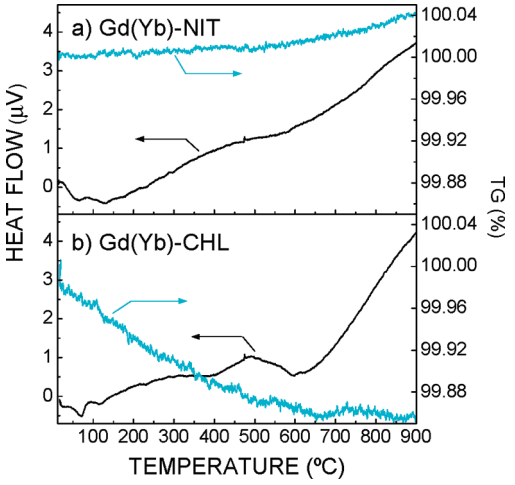

Figure 4. TG (cyan)-DSC (black) curves of hydrothermal $NaGd_{0.95}Yb_{0.05}(WO_4)_2$ prepared at T = 170 °C, pH 7.5, and t = 8 h: (a) using Gd(Yb)-NIT, and (b) using Gd(Yb)-CHL.

WO_4^{2-} group $\nu_1 = 931\ cm^{-1}$, $\nu_2 = 325\ cm^{-1}$, $\nu_3 = 838\ cm^{-1}$, and $\nu_4 = 325\ cm^{-1}$.[25] Broad bands centered at 1630 and ~3440 cm^{-1}, which are seen in both HT materials with a similar intensity, correspond to OH^- stretching vibrations and to HOH bending modes of lattice water, respectively,[25] but since they are also observed in the blank KBr pellet, we can suppose that they are related to a large extent with the used KBr. However, these IR spectra exhibit a significant difference, namely the sharp peak at 1385 cm^{-1} for $NaGd_{0.95}Yb_{0.05}(WO_4)_2$ from Gd(Yb)-NIT, which is attributed to the antisymmetric ν_3 mode of surface-adsorbed NO_3^-.[26,27] The absence of the characteristic peaks of the vibration modes of the CO_3^{2-} group[25] allows discarding any significant reaction with atmospheric CO_2 of prepared samples from both HT synthetic procedures.

TG-DSC curves between 15 and 900 °C for $NaGd_{0.95}Yb_{0.05}(WO_4)_2$ prepared from both Gd(Yb)-NIT and CHL routes (T = 170 °C, pH 7.5, t = 8 h) appear in Figure 4. Small endothermic peaks up to ~130 °C in DSC curves correspond to the removal of some adsorbed water from the surface of the particles, and the other endothermic effects more clearly seen for the CHL-material at ~400 and ~630 °C are due to the loss of coordination hydroxyl groups in the crystal lattice.[28] From TG curves and within the range 15−650 °C, whereas for the NIT material no appreciable mass variation can be detected, there is a ~0.5% weight loss for CHL-$NaGd_{0.95}Yb_{0.05}(WO_4)_2$. In fact, this observed weight drop, and consequently the current amount of water and hydroxyl groups in our HT double tungstate samples, is considerably smaller than for the micrometer-size hydrothermal (180 °C, 48 h) hydroxyl precursor of the isostructural Eu^{3+}-doped $NaY(WO_4)_2$, estimated as a 4% of the initial mass.[29]

(25) Nakamoto, K. *Infrared and Raman Spectra of Inorganic and Coordination Compounds*; Wiley-Interscience: New York, 1986.
(26) Tanner, P. A.; Fu, L.; Cheng, B. M. *J. Phys. Chem. C* **2009**, *113*, 10773.
(27) Tanner, P. A.; Fu, L. *Chem. Phys. Lett.* **2009**, *470*, 75.
(28) Kim, J. M.; Chang, S. M.; Kong, K.-S.; Kim, J.; Kim, W.-S. *Ceram. Int.* **2009**, *35*, 1015.
(29) Lei, F.; Yan, B.; Chen, H. H.; Zhao, J. T. *Inorg. Chem.* **2009**, *48*, 7576.

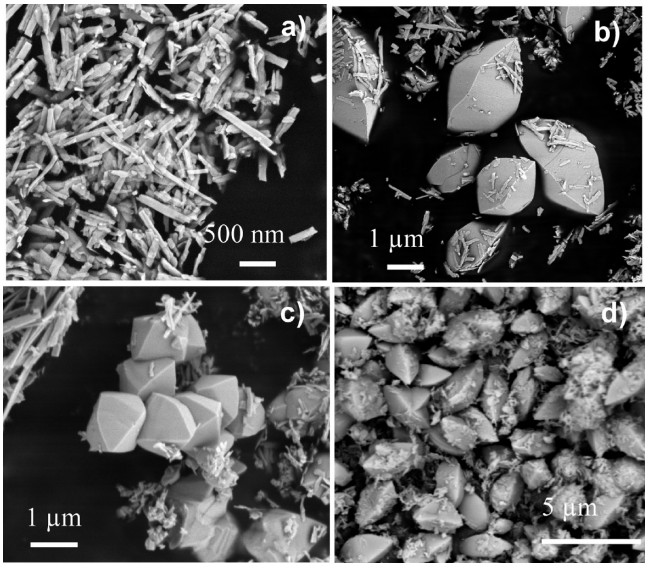

Figure 5. FE-SEM images of $NaGd_{0.95}Yb_{0.05}(WO_4)_2$ prepared by HT synthesis at 170 °C and pH 6, using Gd(Yb)-NIT and reaction times of (a) 6, (b) 8, and (c) 9 h, or (d) Gd(Yb)-CHL after 8 h.

pH, Reaction Time, and Starting Reagents as Factors Influencing the Morphology and Size of HT Yb^{3+}-Doped $NaGd(WO_4)_2$ Materials. Morphology and size of HT $NaGd_{1-x}Yb_x(WO_4)_2$ prepared materials have been examined taking in consideration the influence of the factors that differentiate their synthesis, i.e., pH of the reaction medium, time of reaction t, and used reagents. The influence of the temperature has no been considered since analyzed samples were always doped with an Yb^{3+} content $x \leq 0.05$, and thus all of them prepared at ~170 °C. The results will be arranged as a function of the pH of the starting dispersion.

A. Reaction Media with pH 6.0. Figure 5a−c shows FE-SEM images of the shape evolution with the time (6, 8, and 9 h, respectively) for $NaGd_{0.95}Yb_{0.05}(WO_4)_2$ prepared at pH 6 from Gd(Yb)-NIT, and Figure 5d corresponds to the pure tetragonal phase obtained from Gd(Yb)-CHL at pH 6 after 8 h. It can be observed that the product obtained at the shortest time, 6 h, presents rodlike morphology, which after prolonging the reaction evolves first to ~2.5 μm grain ricelike particles and then to ~1.5 μm distorted octahedra, although rods coexist.

The corresponding TEM images of the crystalline nanorods appearing in syntheses at 170 °C for pH 6 are displayed in Figure 6. Panels 6a−c correspond to products from Gd(Yb)-NIT, in which along the nanorods yielded after the shortest reactions, 6 h, Figure 6a, some quasi-spherical smaller nanoparticles of ~5−40 nm can be also distinguished, Figure 6b, whereas when the reaction is continued for 8 h, the nanorods adquire quite uniforme widths, ~90 nm, Figure 6c, and the smaller nanoparticles completly disappear. Images d and e in Figures 6 correspond to the pure tetragonal phase obtained from Gd(Yb)-CHL after 8 h, where nanorods are very similar to those obtained from Gd(Yb)-NIT after 6 h, whereas the quasi-spherical nanoparticles are currently smaller.

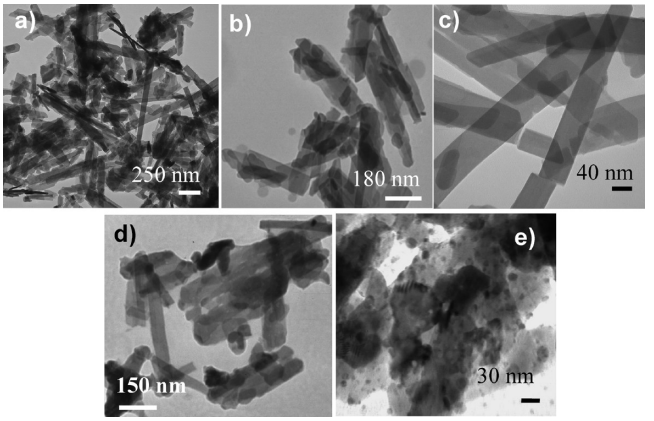

Figure 6. TEM images of $NaGd_{0.95}Yb_{0.05}(WO_4)_2$ prepared by HT synthesis at 170 °C and pH 6, using Gd(Yb)-NIT and reaction times of (a, b) 6 or (c) 8 h, or (d, e) Gd(Yb)-CHL after 8 h.

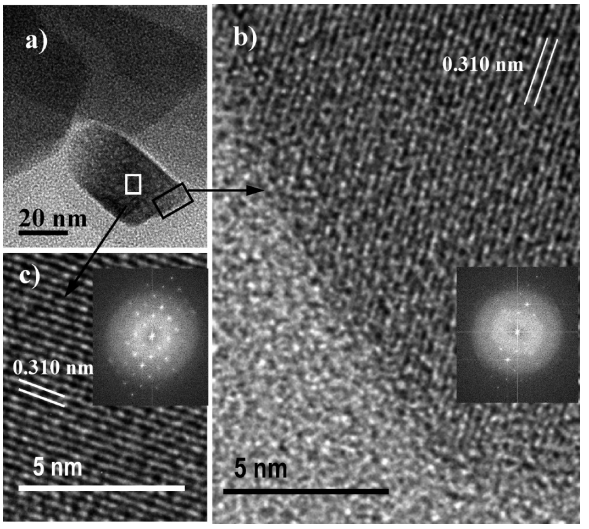

Figure 7. TEM, HRTEM, and FFT images of selected areas in nanorods of $NaGd_{0.95}Yb_{0.05}(WO_4)_2$ prepared by HT synthesis at 170 °C and pH 6, using Gd(Yb)-NIT and reaction time of 8 h.

Further insight into the structures of the previous nanorods was afforded by HRTEM. Images displayed in Figure 7 correspond to nanorods from Gd(Yb)-NIT, pH 6, and $t = 8$ h (as these in Figure 6c). Selected areas in a nanorod were at its end, image in Figure 7b, and a well-inside section, image in Figure 7c. Fast Fourier Transform (FFT) images are included as insets in each case. The observed lattice fringe distances of the two selected areas are 0.310 nm, which match the (112) interplanar spacing of $NaGd_{0.95}Yb_{0.05}(WO_4)_2$.[8] However, HRTEM and FFT images suggest that the central area is more crystalline and has higher structural uniformity than at the edge.

The Figure 8 shows a representative HRTEM image of rods from Gd(Yb)-CHL, pH 6 and $t = 8$ h (i.e., as these in images d and e in Figure 6). The observed lattice fringe distances are 0.470 nm, which corresponds to the (011) interplanar spacing of tetragonal $NaGd_{0.95}Yb_{0.05}(WO_4)_2$. A slight misorientation between sets of these planes has been highlighted at the upper left side of Figure 8b, suggesting the presence of coalescent primary nanoparticles to constitute the nanorods.

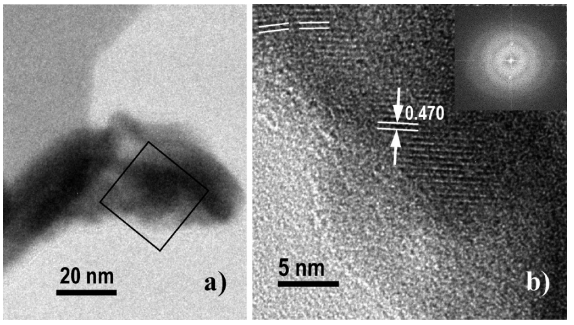

Figure 8. (a) TEM and (b) HRTEM and FFT images of $NaGd_{0.95}Yb_{0.05}(WO_4)_2$ prepared by HT synthesis at 170 °C and pH 6, using Gd(Yb)-CHL and $t = 8$ h.

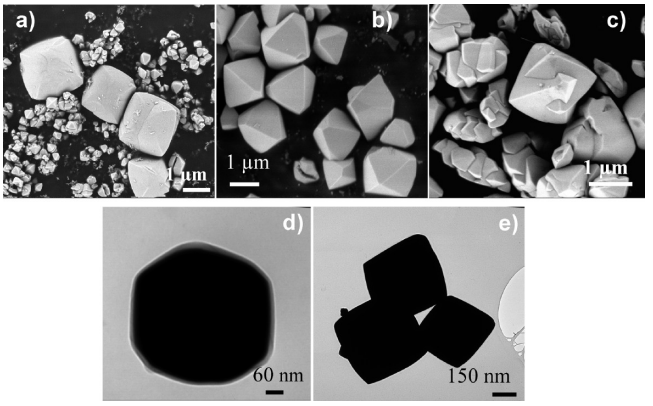

Figure 9. Images of $NaGd_{0.95}Yb_{0.05}(WO_4)_2$ particles prepared by HT synthesis at 170 °C and pH 7.5 using Gd(Yb)-NIT: FE-SEM micrographs for reaction times of (a) 8, (b) 12, and (c) 14 h; TEM views of the smaller octahedra obtained after reactions lasting (d, e) 8 h.

B. Reaction Media with pH up to 7.5. When the pH is raised to 7.5, syntheses carried out with Gd(Yb)-NIT at 170 °C and 8−9 h produce crystalline pseudo-octahedral particles, with a nearly double distribution of sizes, i.e., ~2.5 μm for the larger and ~400 nm the smaller ones, with the nanorods obtained under pH 6 no longer being detected in the current preparation. When the reaction continues up to 12 h, only better-formed ~1.5 μm octahedra constitute the HT product, which for longer reaction times seem to evolve to rows constituted by interpenetrated octahedra. Figures 9a−c show representative FE-SEM images of the time-dependent shape of the materials prepared using Gd(Yb)-NIT dispersions at pH up to 7.5, and Figure 9d,e displays TEM micrographs of the smaller crystalline octahedra.

Alternatively, for reactions with Gd(Yb)-CHL reagents at pH 7.5 lasting 8 h, the aspect of the HT material is quite similar to that obtained at pH 6, that is, large ~2.5 μm grain ricelike and pseudo-octahedral particles as well as irregular nanorods, with the former shapes prevailing over nanorods, see the Figure 10a. Finally, when the reaction is prolonged to 14 h, the nanorods disappear, and rice grainlike and pseudo-octahedral particles, again with a nearly double distribution of sizes, are observed, Figure 10b. Crystalline octahedral particles are getting somewhat smaller and with a better defined shape for long lasting reactions, in a manner similar to that previously stated for HT materials from Gd(Yb)-NIT dispersions.

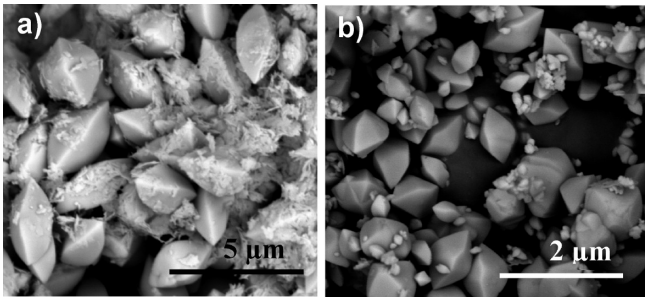

Figure 10. FE-SEM images of $NaGd_{0.95}Yb_{0.05}(WO_4)_2$ particles prepared by HT synthesis at 170 °C and pH = 7.5 using Gd(Yb)-CHL, for reaction times of (a) 8 and (b) 14 h.

The close inspection of FE-SEM, TEM and HRTEM images in Figures 5−10 allows the identification of some specific details that differentiate the morphologies and sizes of HT Yb-$NaGd(WO_4)_2$ according to the experimental synthetic procedure. Even if none individual factor (pH, starting reagents, time of reaction t, pH, or temperature) completely determines the morphology, when the influence of the used lanthanide reagent is considered it seems that the larger particles obtained after $t \geq 8$ h have a bit different shape, which for HT materials from Gd(Yb)-NIT is always close to more or less imperfect octahedra, Figures 5c and 9a,b, whereas those from Gd(Yb)-CHL would be better described as resembling grains of rice, Figures 5d and 10a,b. Furthermore, the nanorods yielded for $t \leq 8$ h seem to be more irregular, with rougher aspect, for the material prepared using Gd(Yb)-CHL than for the Gd(Yb)-NIT counterpart, see corresponding TEM images d and b in Figure 6. On the other hand, also depending on the used lanthanide reagent, the same observed sequence of morphologies, namely quasi-spherical nanoparticles, nanorods, nanorods accompanied by larger particles (pseudo-octahedra and rice grainlike), and larger particles with a double distribution of sizes, appear after different t; the sequence of shapes of HT materials obtained using Gd(Yb)-CHL is "delayed" with regards to that corresponding to Gd(Yb)-NIT reagents, and some examples are that the presence of quasi-spherical nanoparticles is observed up to $t = 6$ h for materials from Gd(Yb)-NIT and with $t = 8$ h using Gd(Yb)-CHL reagents as well as the double distribution of sizes for larger particles appear with $t = 8$ h in the former syntheses and with $t = 14$ h using the latter reagents. Furthermore, although rows of interpenetrate octahedra have been seen as the final crystallized forms only from Gd(Yb)-NIT, Figure 9c, it can be reasonably supposed that they constitute the last step of the above sequence of shapes adopted by HT crystalline particles of the pure tetragonal phase of Yb-$NaGd(WO_4)_2$. However, the factor having the predominant influence in the stability (see XRPD patterns in Figures 1b,c and 2a−c) as well as in the shape of the tetragonal phase of the HT double tungstate is the pH of the starting dispersion. Concerning this aspect, even if the presence of nanorods or micrometersized crystals is dominant but not fully determined by adjusting the pH in the slightly acid to slightly basic range, the remaining experimental conditions can always be adequately combined to finely tune the achievement of the desired morphology.

Concerning the mechanism of formation of particles in current HT processes, we can assume that the time-dependent evolution of particles starts with the development of small crystalline nuclei (as those shown in Figure 6e, responsible for the broadened XRPD pattern in Figure 1b1) from the amorphous fine particles present in the highly supersaturated dispersion. Then, in a first step, the small crystals can redissolve and larger crystals, nanorods, will grow at their expense until the consumption of the solute species. In the early stages of this process, there is a coexistence of irregular nanorods and nanoparticles, as shown in Figure 6b; when the reaction continues, nanoparticles vanish and the nanorods become regular and longer, suggesting that longer nanorods grow at the cost of the smaller particles. Similar characteristics have been described for the growth and evolution of crystalline nanorods of transition metals single tungstates, also prepared by HT procedures,[30] and in this case, the proposed growth mechanism is based in a spherical diffusion model that takes into account the structural characteristics of the studied monoclinic tungstates. However, the possibility of aggregation or coalescence of nanoparticles having a suitable crystallographic orientation to give a larger crystal should be also considered. In this kind of mechanism, usually named "oriented attachment",[31,32] the initial small particles are not necessarily well-oriented at the first moment. Instead, they can form an agglomerate and then align by reorientation[33] in such a way that the secondary particles can present regions with an important preferred orientation of the initial nanocrystals, or they can even be new single crystals produced by an irreversible attachment of highly oriented nanocrystals. This mechanism has been reported as relevant for particles freely moving in solution, and especially when they have abundant surface-bound water, i.e., in hydrothermal processes. In fact, an oriented attachment was indicated as the origin of the formation of scheelite single crystalline dendrites of $PbMoO_4$ from nanoparticles in its hydrothermal synthesis.[34] In the current case, the images of the material from Gd(Yb)-CHL at pH 6 after 8 h, as shown in Figures 6d and 8b, would able to sustain this oriented aggregation mechanism for the growth of the observed HT nanorods.

On aging for longer periods, HT syntheses generate the usually described more o less complex pseudo-octahedral morphologies of the micrometersize crystals of tetragonal double tungstates with scheelite structure.[35]

(30) Yu, S.-H.; Liu, B.; Mo, M.-S.; Huang, J.-H.; Liu X.-M.; Qian, Y.-T. *Adv. Funct. Mater.* **2003**, *13*, No. 8, 639.
(31) Penn, R. L.; Banfield, J. F. *Science* **1998**, *281*, 969.
(32) Penn, R. L. *J. Phys. Chem. B* **2004**, *108*, 12707.
(33) Tiemann, M.; Marlow, F.; Hartikainen, J.; Weiss, O.; Lindén, M. *J. Phys. Chem. C* **2008**, *112*, 1463.
(34) Chen, Y.; Wang, Y.; Chen, D.; Bao, F. *J. Phys. Chem. B* **2005**, *109*, 794.
(35) Byrappa K. M. Yoshimura M. Hydrothermal Synthesis and Crystal Growth of Fluorides, Sulfides, Tungstates, Molybdates and Related Compounds. In *Handbook of Hydrothermal Technology*; Noyes Publications: Park Ridge, NJ, 2001; pp 636−646.

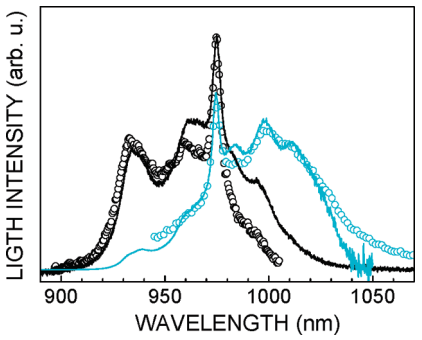

Figure 11. Excitation (black circles, $\lambda_{EMI} = 1020$ nm) and emission (cyan circles, $\lambda_{EXC} = 934$ nm) spectra of hydrothermal $NaGd_{0.99}Yb_{0.01}(WO_4)_2$ material at 300 K. The 300 K averaged $(2\sigma + \pi)/3$ absorption (black line) and emission (cyan line) cross-sections of Yb^{3+} in $NaGd(WO_4)_2$ single crystal are given for comparison.

Spectroscopic Characterization of HT Yb^{3+}-Doped $NaGd(WO_4)_2$ Materials. The Yb^{3+} optical absorption and photoluminescence arise from the electronic transitions between the ground $^2F_{7/2}$ multiplet to the excited $^2F_{5/2}$ one. These multiplets are composed of 4 and 3 doubly degenerate Stark levels labeled as $^2F_{7/2}(0,1,2,3)$ and $^2F_{5/2}(0,1,2)$, respectively. Figure 11 shows the room-temperature emission and excitation (formally equivalent to the optical absorption) spectra of HT $NaGd_{0.99}Yb_{0.01}(WO_4)_2$ dispersed in EG. These spectra are compared to the average $(2\sigma + \pi)/3$ polarized absorption and emission cross-sections of Yb^{3+} in a $NaGd(WO_4)_2$ single crystal.[8,9] Apart from differences in absolute intensities arising from the different spectral response of the exciting MOPO system, the fluorescence spectrometer as well as of the absorbance spectrophotometer, the observed transition bands for HT $NaGd_{0.99}Yb_{0.01}(WO_4)_2$ and for the Yb-doped $NaGd(WO_4)_2$ single crystal show very similar features, i.e., the same energies and band shape. This indicates that Yb^{3+} is actually incorporated in $NaGd_{1-x}Yb_x(WO_4)_2$ particles, and none segregated Yb-containing phase such as the cubicYb_2O_3 (with a distinctively much stronger crystal field and therefore larger $^2F_{5/2}$ spectral splitting) contributes to the spectra.

Yb^{3+} operates as a quasi−three level laser system. Pump power threshold and inversion population are related to the $^2F_{5/2}$ lifetime value, but the experimental measurement of this parameter is quite complex. Because of the non-negligible electronic population of the low energy terminal level, often $^2F_{7/2}$ ($n \neq 0$), the self-absorption of the photoluminescence and its re-emission leads to an artificial enlargement of light decays.[36] This effect is already noticeable for [Yb] higher than 1 mol %. On the other hand, some discussion exists about the possibility of concentration quenching for Yb^{3+}, and in fact it is often found that the $^2F_{5/2}$ lifetime decreases with increasing [Yb]. However, the lifetime measured for the stoichiometric $Yb_3Al_5O_{12}$ and for < 10 at % Yb-doped $Y_3Al_5O_{12}$ single crystals prepared by using very high purity chemicals and selected crucibles has been found to be similar, that points to residual impurities as the origin of the lifetime decrease.[18,19] Finally, the Yb^{3+} lifetime in nanoparticles with size < 100 nm is further affected by the non-negligible effect of the surface as well as by the possible change of the effective refractive index of the compound due to the surrounding immersion medium.[37]

To assess any difference in the Yb^{3+} lifetime in our HT synthesized particles with regard to bulk single crystals, we have monitored at 300 K the luminescence decay after excitation at $\lambda_{EXC} = 940$ nm with a narrow-band MOPO system. To minimize changes originated by the medium surrounding the nanoparticles, HT $NaGd_{1-x}Yb_x(WO_4)_2$ samples were dispersed in fluids having a high refractive index. For this purpose we used either EG ($n = 1.52$) or FL ($n = 1.94$). Because the refractive index of the latter closely matches that of the studied $NaGd(WO_4)_2$ bulk crystal, $n = 1.945$ at $\lambda = 1000$ nm,[8] any modification of the radiative properties of Yb^{3+} incorporated in nanoparticles can be ruled out by using it, making unnecessary the corrections due to the "filling factor" reported for nanoparticles lifetime measurements.[37,38] Thus, by comparing the lifetimes obtained using EG or FL dispersions, one can estimate, at least qualitatively, the effect of the surrounding media. Furthermore, the procedure followed to minimize the above indicated lifetime lengthening effect due to self-absorption and its subsequent re-emission consists in carrying out sequentially measurements in dispersions with getting smaller amounts of $NaGd_{1-x}Yb_x(WO_4)_2$ until the lifetime remains constant or the detection limit was reached. In each case, the measurement was repeated several times.

We first analyze the results of Gd(Yb)-NIT (99.99%) syntheses at pH 7.5 for $t > 8$ h. These conditions lead to a well-defined distribution of micrometersized pseudo-octahedra and nearly no presence of nanoparticles. Figure 10 shows the light decays obtained at $\lambda_{EMI} = 990$ nm after excitation at $\lambda_{EXC} = 940$ nm. For most of these HT materials the decays are well fitted by single exponential functions. The lifetime obtained for the samples with the lowest [Yb], $NaGd_{0.999}Yb_{0.001}(WO_4)_2$, is $\tau = 335 \pm 10$ μs, i.e., similar to that obtained in the single crystal.[8] For this reagent purity, the increase of the Yb^{3+} concentration shortens the observed lifetime, compare Figure 12a with Figure 12b, c, but still a single exponential decay is observed.

HT synthesis with both acid pH 6 medium and Gd(Yb)-CHL as reagents favors the formation of nanoparticles and nanorods and their coexistence with micrometer-sized pseudo-octahedra. Figure 13 shows the photoluminescence light decays for the products obtained under these conditions. Now the decays can not be fitted to a single exponential function, and only the long-time tail behaves as single exponential, but the contribution of faster decay

(36) Auzel, F.; Baldacchini, G.; Laversenne, L.; Boulon, G. *Opt. Mater.* **2003**, *24*, 103.

(37) Meltzer, R. S.; Feofilov, S. P.; Tissue, B.; Yuan, H. B. *Phys. Rev. B* **1999**, *60*, 14012.

(38) Liu, G.; Chen, X. Spectroscopic Properties of Lanthanides in Nanomaterials. In *Handbook on the Physics and Chemistry of Rare Earths*; Gschneidner, K. A., Jr., Bünzli, J.-C. G., Pecharsky, V. K., Eds.; Elsevier B.V.: Amsterdam, 2007; Vol. *37*, chapter 233.

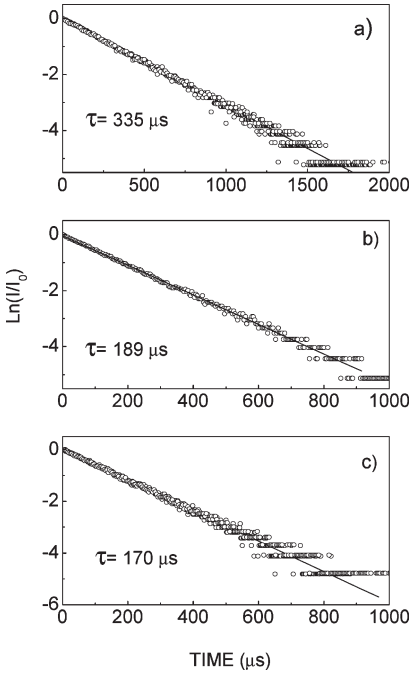

Figure 12. Photoluminescence intensity decays of the emission at λ_{EMI} = 990 nm (λ_{EXC} = 940 nm) of Yb^{3+} in HT $NaGd_{1-x}Yb_x(WO_4)_2$ prepared at pH 7.5 by using nitrate reagents, (a) $NaGd_{0.999}Yb_{0.001}(WO_4)_2$, t = 8 h; (b) $NaGd_{0.95}Yb_{0.05}(WO_4)_2$, t = 9 h; (c) $NaGd_{0.95}Yb_{0.05}(WO_4)_2$, t = 14 h. In all cases, the samples were dispersed in EG.

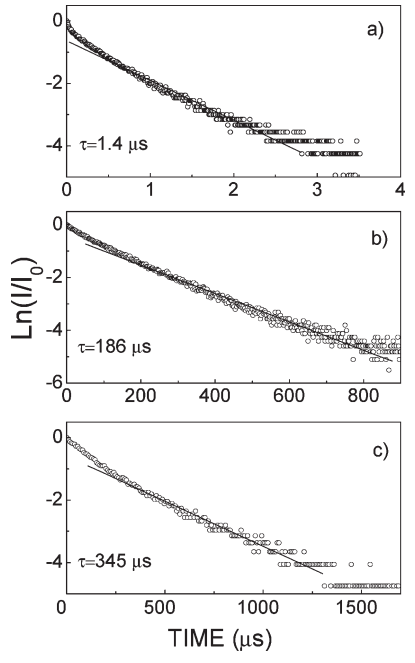

Figure 13. Photoluminescence intensity decays of the Yb^{3+} emission at $\lambda_{EM\ I}$ = 990 nm (λ_{EXC} = 940 nm) in HT $NaGd_{1-x}Yb_x(WO_4)_2$ prepared by using chlorides, a) $NaGd_{0.95}Yb_{0.05}(WO_4)_2$, pH 6, t = 3 h; (b) $NaGd_{0.95}Yb_{0.05}(WO_4)_2$, pH 6, t = 8 h; (c) $NaGd_{0.995}Yb_{0.005}(WO_4)_2$ pH 7.5, t = 8 h. Particles dispersed in (a, b) EG or (c) FL.

regimes is evident. For pH 6 and very short t (3 h), nanoparticles and nanorods display very short lifetime, 1.4 μs. Such lifetime reduction with regards to that obtained in single crystals or in the monodisperse distribution of pseudo-octahedra must be attributed to the large influence of the surface defects on the radiative

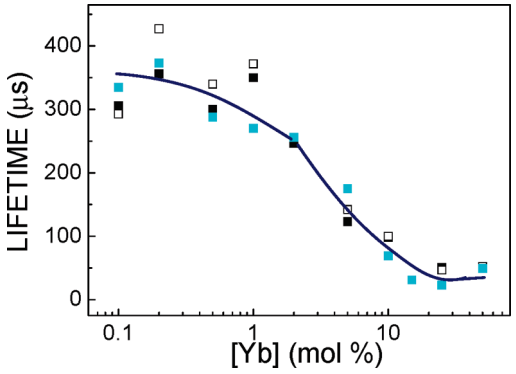

Figure 14. Room-temperature $^2F_{5/2}$ lifetime (λ_{EXC} = 940 nm, λ_{EMI} = 990 nm) of Yb^{3+} in HT $NaGd_{1-x}Yb_x(WO_4)_2$ obtained with Gd(Yb)-NIT (cyan symbols) or Gd(Yb)-CHL (black symbols) reagents. In both cases the purity Yb_2O_3 was 99.99%. Samples dispersed in ET (full symbols) or in FL (open symbols). The solid line is a visual help to show the data evolution.

properties of Yb^{3+}. For longer t (8 h) at pH 6, or by raising the pH up to 7.5, the Yb^{3+} lifetime of HT materials from Gd(Yb)-CHL reagents show fast and slow components, which could be attributed to the coexisting nanorods and microoctahedra, respectively. Furthermore, when [Yb] became lower values from the slow component increase up to consistency with those observed in the single crystal, i.e., 345 μs for $NaGd_{0.995}Yb_{0.005}(WO_4)_2$.

From now we shall only consider the long time regime of the photoluminescence decays, i.e., the contribution associated to micrometer-sized pseudo-octahedra. Figure 14 shows the evolution of the Yb^{3+} lifetime with [Yb] for both Gd(Yb)-CHL and Gd(Yb)-NIT preparations. The observed lifetime reduction when [Yb] becomes higher indicates that the self-absorption and re-emission does not dominate the measurement, otherwise the measured lifetime would increase. The near to constant or even subtle enlargement of the lifetime observed in Figure 14 from 25 to 50% mol [Yb] may indicate that the first value is the threshold concentration from which the self-absorption of the fluorescence can not be avoided by the particle dispersion, whose limit is imposed by the detection sensitivity. The difference found between lifetime values for dispersions in EG or in FL is not very relevant, even basically inexistent for $[Yb^{3+}] \geq$ 2%mol, as expected due to the micrometer size of the octahedra. Also, lifetimes for both preparations are quite similar, indicating that each determined lifetime is always representative of the material properties, and that this is not deeply influenced by the preparation method.

Next, we wanted to investigate whether the lifetime reduction observed in Figure 14 is an intrinsic behavior of Yb^{3+} or if it is associated with the presence of unwanted impurities.[18,19] For this purpose we have synthesized $NaGd_{1-x}Yb_x(WO_4)_2$ compositions with x = 0.05, 0.1, 0.25, and 0.5 via Gd(Yb)-CHL reagents for which the raw Yb_2O_3 oxide has purity levels ranging from 99.9 to 99.9999%. Figure 15 shows the results obtained for each composition prepared through Yb_2O_3 with several purities. These results demonstrate that for 5 and 10% mol [Yb] the lifetime significantly increases by using Yb_2O_3 with purity higher than 99.99%, although only in the first

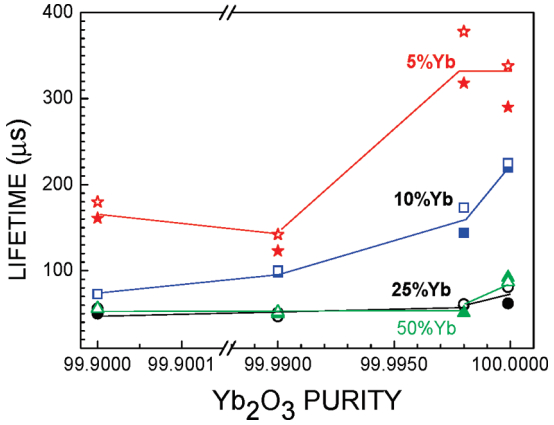

Figure 15. Room-temperature $^2F_{5/2}$ lifetime (λ_{EXC} = 940 nm, λ_{EMI} = 990 nm) of Yb^{3+} in HT $NaGd_{1-x}Yb_x(WO_4)_2$ obtained using Gd(Yb)-CHL reagents as a function of the purity of the raw Yb_2O_3 oxide: x = 0.05, stars; x = 0.1, squares; x = 0.25, circles, and x = 0.50, triangles. Samples dispersed in EG (full symbols) and in FL (open symbols). Solid lines are visual helps to show the evolution of data.

case the lifetime reaches the reference value obtained in single crystals.[8] For 25 and 50% mol [Yb] only the highest Yb_2O_3 purity, 99.9999%, produced a slight lifetime enlargement, an indication of that the lifetime decrease observed for high Yb^{3+} contents is not an intrinsic property of the Yb^{3+} the material, but it must be rather associated to the presence of other impurities able to interact with Yb^{3+}, like the close electronic configurations of Tm^{3+} or Er^{3+}. The fact that the lifetime is not fully recovered even for the 99.9999% Yb_2O_3 prepared products must be associated to the current purity level of the other used reagents, mainly 99.99% Gd_2O_3.

Conclusions

Low-temperature (170−200 °C) and autogenous pressure HT preparations using nitrate and chloride reagents as Gd and Yb sources lead to the synthesis of $NaGd_{1-x}Yb_x(WO_4)_2$ ($0.001 \leq x \leq 0.5$) particles with tetragonal scheelite-like structure phase. Nearly neutral pH ~7.5 conditions ensure the widest range of reaction times while keeping the stability of the wanted tetragonal phase. The use of a slightly acid dispersion requires a more careful control of the reaction to obtain the pure phase.

Although synthetic routes with both kind of reagents yield basically the same particle morphology sequences, the presence of nanoparticles is more evident when using Gd(Yb)-CHL, whereas the faster growth rate favors well-defined micrometer-sized octahedral particles when Gd(Yb)-NIT is used. Of interest for their incorporation in 2D micropatterned hybrid laser composites are the robust and solid morphologies, like the interpenetrated rows of octahedra that can be provided by HT treatments.

The spectroscopic properties of Yb^{3+} in $NaGd_{1-x}Yb_x(WO_4)_2$ HT synthesized micrometer-sized octahedra are equivalent to those obtained in bulk single crystals, i.e., Yb^{3+} optical transitions with very similar energy and band shape, as well as a single exponential photoluminescence decay and $^2F_{5/2}$ lifetime $\tau \approx 330$ μs for $0.001 \leq x \leq 0.005$ doped samples. The nanoparticles and nanorods formed with Gd(Yb)-NIT and pH < 7 by short time (t < 8 h) annealing, and in Gd(Yb)-CHL preparations show a strong reduction of the Yb^{3+} lifetime with regards to that observed in micrometer-sized octahedra or in single crystals, leading to nonexponential fluorescence decays when both nano- and micrometer-sized particles coexist.

For the title materials, the Yb^{3+} lifetime increases toward its radiative value when raw Yb_2O_3 with increasing purity level is used in the HT processes. These results indicate an easy an effective way to incorporate larger concentrations of Yb^{3+} in laser elements prepared with the described materials.

Acknowledgment. This work was supported by the Spanish Project MAT2008-06726-C02-01